SEMIANNUAL STATUS REPORT

FOR THE PERIOD 1 JANUARY 1966 THROUGH 30 JUNE 1966

Required under the terms of NASA Research Grant NsG 443

"Research Related to an Experimental Test of General Relativity"

Under the Direction of
H. Knoebel and D. Alpert

COORDINATED SCIENCE LABORATORY

University of Illinois
Urbana, Illinois

July, 1966

Gyro Materials

Considerations of torques due to 1) a fixed charge on a sphere in an electric field, 2) induced currents in a conductive sphere rotating in a magnetic field, and 3) induced currents in a conductive sphere rotating in an electric field have established a range of material electrical resistivity of $10^3 < \rho_e$ 10^{10} ohm cm. By using a passive temperature stabilization technique of controlling the solar absorptivity α to thermal emissivity ϵ of multilayer coatings on the satellite gyro,[1,2] a desired operating temperature range between the approximate temperature limits -80°C to 100°C can be engineered. Since the operating temperature has not yet been established, a search for materials which have acceptable electrical resistivity within the above temperature limits has been instituted. The materials germanium, silicon, and titanium dioxide, when properly doped, and certain glasses are among a number which appear to satisfy the electrical resistivity requirements. A sodium silicate glass,[3] composed of 60% Si O_2, 30% Na_2 0, and 10% Ca 0 has measured resistivities of 3×10^6 ohm cm at 50°C and 5×10^2 ohm cm at 300°C. Extrapolating by means of a best fitting curve given by $\rho = \rho_o e^{\alpha/T}$ where ρ is the resistivity, T the absolute temperature, and ρ_o and α are

---

[1] Hass, G., Drummeter, L., and Schach, M., "Temperature Stabilization of Highly Reflecting Satellites," Journ. Opt. Soc. Am. 49, (September, 1959) pp. 918-924.

[2] Symposium on Thermal Radiation of Solids, ed. by S. Katzoff (March 4-6, 1964) NASA, Sp-55.

[3] Goldsmith, A., Waterman, T.E., Hirschorn, H. J., Handbook of Thermophysical Properties of Solid Materials, Vol. II: Ceramics (The MacMillan Co., New York, 1961) VII-C-1-b.

constants, the upper resistivity limit of 10^{10} ohm cm is obtained at -40^{o}C. The lower limit of 10^{3} ohm cm is obtained at 270^{o}C. Hence, a satellite made of this glass could operate at any given temperature between -40^{o}C and 270^{o}C.

In addition, these materials must satisfy other properties, one of the most important being high mechanical damping. After launch and gyro spin-up and after any micrometeorite cratering, the gyro angular momentum vector, instantaneous spin vector, and symmetry axis vector will not in general be aligned. The inherent damping, in which elastic vibrations due to gyroscopic action cause energy dissipation and consequent realignment of these vectors, will be used. A good approximation for the time required for the gyro symmetry axis vector to align itself from an initial angle θ_i to a final angle θ_f with respect to the angular momentum axis is given by[4]

$$T = (2\pi C\omega_o/\gamma W)\, \ell n(\theta_i/\theta_f) \qquad (1)$$

where C is the gyro polar moment of inertia, ω_o is the gyro spin frequency, γ is the damping factor defined by the fraction of the elastic energy dissipated to the amount of energy stored per cycle, and W is the total elastic strain energy of the gyro.

The more familiar and common term Q will be used to replace the damping factor γ by the relation $Q = 2\pi/\gamma$. For conditions of this experiment, a 12-inch diameter gyro rotating at 100 H, approximate

---

[4]Thompson, W. T. and Reiter, G. S., "Attitude Drift of Space Vehicles," J. Astronaut. Sci., 7 29-34 (1960).

calculations of W indicate that for damping times T of about half a day, with $\theta_i \approx 5^o$ and $\theta_f = 0.1$ arc second, a value of 1/Q larger than about 5×10^{-3} is required. More exact calculations of W are now being undertaken.

Among the more promising high damping factor materials are the glasses. Among other things, 1/Q is a function of the elastic vibrating frequency which, for the gyro, is given by $[(A-C)/A]\omega_o \cos\theta$. Present gyro parameters indicate a vibration frequency of about 1 to 3 Hz. Glass has a maximum value for 1/Q of about 4×10^{-3} in this range of frequencies[5,6,7] and at room temperature. At -100^oC the value drops to about 2×10^{-3}.

In order to check this result, a four-foot torsional pendulum consisting of a fine strand of pyrex glass was constructed within a vacuum chamber and the logarithmic decrement $\delta = \pi/Q$ was measured at room temperature. The natural frequency of the pendulum was about 0.3 Hz, at which a measured value of .0043 for 1/Q was obtained, as compared with a value of .004 at the same frequency from reference 5. Hence, it appears that a glass gyro rotor can satisfy the damping requirement and possibly the resistivity requirement. The latter will be checked by measuring a sample of the glass.

---

[5] Zener, C., Elasticity and Anelasticity of Metals, (University of Chicago Press, 1948) p. 55.

[6] Bennewitz, K. and Rötger, H., "Uber die Innere Reibung fester Körper; Absorptionsfrequenz von Metallen in akustischen Gebiet," Phys. Zeitschr., 37, 578 (1936).

[7] Forry, K. E., "Two Peaks in the Internal Friction as a Function of Temperature in Some Soda Silicate Glasses," Am. Ceram. Soc., 40, [3], 90-94 (1957).

In order to discover any problems associated with the use of glass under severe centrifugal stress, glass disks were spun to the bursting point in a motor-driven test fixture. According to elasticity theory, the maximum stress for a solid, spinning sphere is at the center and is approximately given by[8]

$$\sigma_{max} = \rho\omega^2 r^2 \left(\frac{3+2\mu}{7+5\mu}\right)$$

where ρ is the density, ω is the angular spin, r is the radius, and μ is Poisson's ratio. For a thin, solid disk, the maximum stress is also at the center and is, to good approximation,

$$\sigma_{max} = \rho\omega^2 r^2 \left(\frac{3+\mu}{8}\right).$$

For glass, $\mu \approx 0.16$ so that the bracketed factors become 0.425 and 0.395 for the sphere and disk, respectively. Hence, the maximum stresses are nearly the same for identical materials, diameters, and spin speed, which justifies the use of disks for this test.

Adequate protection was provided to absorb the energy when the glass structure failed. The glass disks were made of ordinary plate glass window, 12 inches in diameter and 1/8-inch thick. An aluminum spindle was bonded at the center of the glass disk and the resulting structure was checked for balance about the spindle. The first glass disk sample was spun about its attached spindle and the speed slowly increased to 166 rps, at which point the glass disk shattered into small

---

[8] Chree, C., Cambridge Phil. Soc. Trans., Vol. 14, Part 3, (1889), p. 292.

particles. The second sample, which was not balanced as well as the first, failed at 145 rps. The maximum stresses for the disk and sphere spinning at 150 rps are about 3,200 psi and 3,400 psi, respectively. If the spin speed is reduced to 100 rps, the maximum stress for the sphere becomes 1,530 psi since the stress is proportional to the square of the spin rate. These tests tentatively indicate an upper spin speed limit of about 100 rps for the spherical galss satellite, with an adequate safety factor. Further spin tests will be conducted with better balanced disks and with the actual material when it has finally been selected. Further spin tests will be conducted with the actual material when it has been finally selected for its proper volume resistivity at the satellite operating temperature.

Satellite Observation Times and Mirror Normal Angles

A digital computer program has been written to determine typical times of observation of a sunlight-illuminated satellite. At each instant of time the satellite is observable, the following quantities are computed: the slant range and elevation of the satellite, the unit vector normal to a hypothetical mirror on the satellite which will reflect sunlight to the observing station, and the angle of incidence of sunlight on the mirror. On a given pass, an actual observation is predicted if one or more of the satellite's mirror normals lie in the range of the hypothetical values calculated.

Preliminary results show that for an equatorial orbit of 1,000 km altitude, an average of three observations a day may be possible from a tracking station at $\pm$ 16^{o} latitude.

Gas Drag

The work on gas drag reported in the Semiannual Status Report for the period 1 January 1965 through 30 June 1965 has been extended to include the effects of non-uniform heating and orbital regression. This work has been completed and is available from the Coordinated Science Laboratory.[9] When applied to the aerodynamic analysis, the orbital regression analysis reveals the necessary orbital parameters needed to minimize the aerodynamic torque. The non-uniform heating effect is of the same class as surface roughening by dust particles, radiation damage, and other effects which cause localized changes in the surface accommodation coefficient, possibly giving rise to a torque. The non-uniform heating analysis, therefore, provides an example of the precession to be expected from this class of external effects.

The satellite spin axis parallel to the sun line and in the orbital plane, as shown in Fig. 1, was taken as the worst case in calculating the non-uniform heating effect. The half-surface always in the sunlight was assumed to have a uniform temperature and accommodation coefficient higher than the other half-surface not illuminated by the sun's rays. The aerodynamic torque equations in a non-regressing orbit were then employed to find the maximum total angular precession occurring in one year. The precession rate is periodic and the angular deviation of the spin axis varies from zero to a maximum in a period of half a year. The maximum value, shown in Fig. 2, is seen to depend upon the

[9] Karr, G. R., "Aerodynamic Torque on a Spinning Spherical Satellite with Application to Measurement of Accommodation Coefficients," Report R-295, Coord. Science Lab., University of Illinois, Urbana, Illinois, May, 1966.

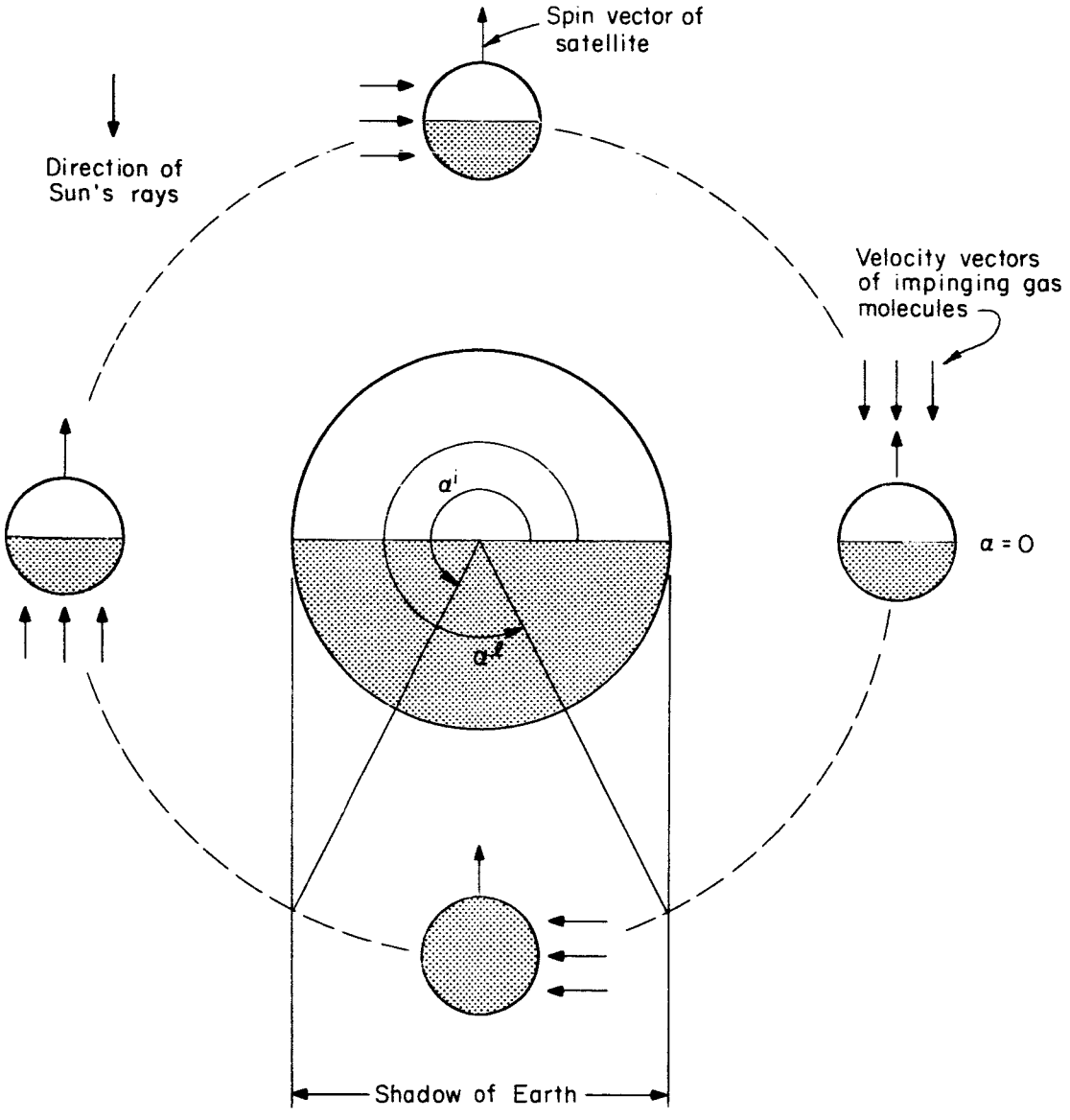

Fig. 1. Diagram of nonuniform solar heating effect for satellite in equatorial orbit.

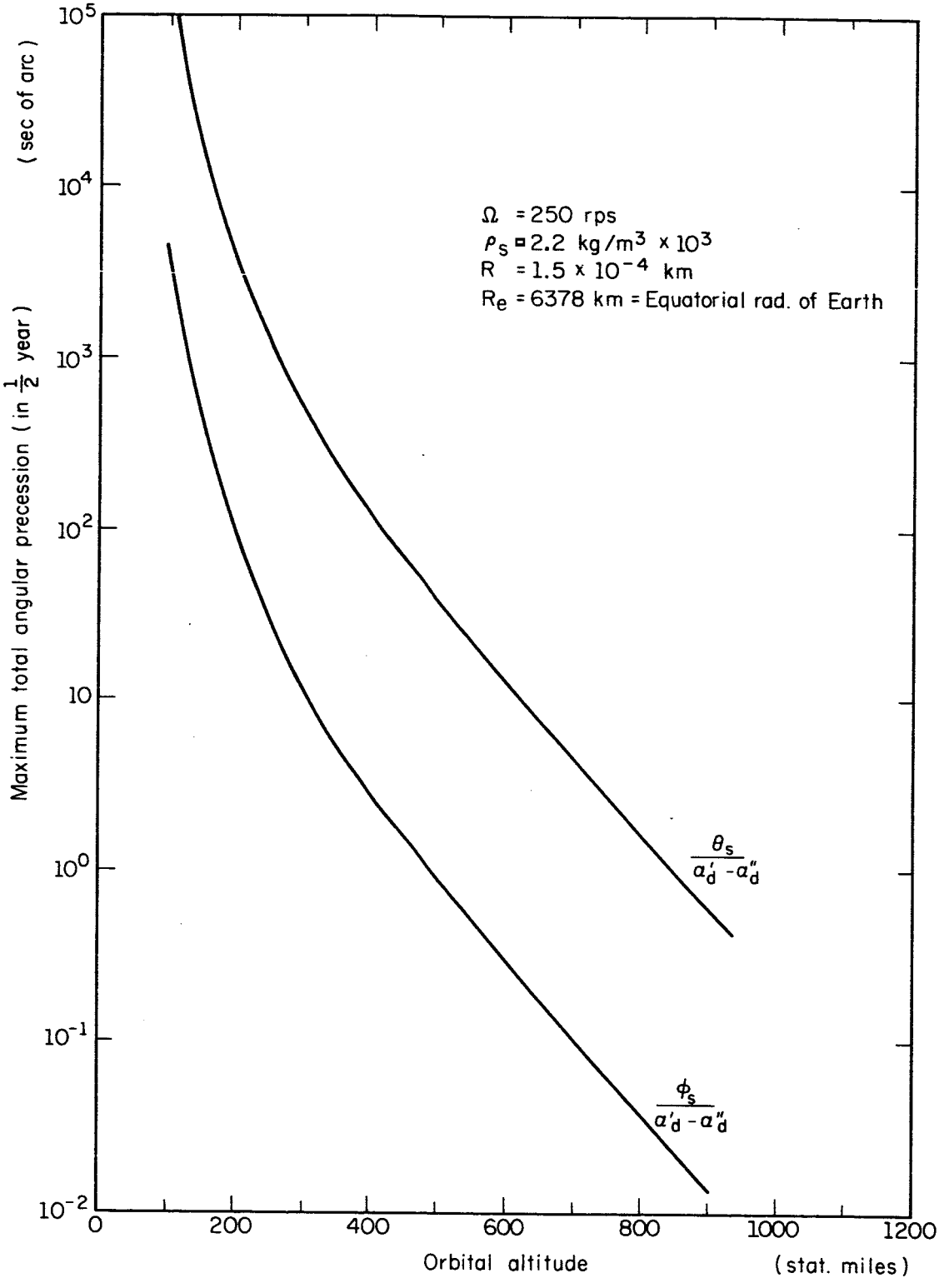

Fig. 2. Aerodynamic precession due to nonuniform solar heating vs. altitude.

accommodation coefficient difference and the orbital altitude. At 600 miles, however, the precession can be kept to less than one-tenth the Schiff effect if the accommodation coefficient difference is less than .01, a value which is reasonable in view of the experimental data available on this effect.

The orbital regression analysis applied to the aerodynamic torque problem results in solutions which are similar to the gravity gradient analysis. The solutions are separable into two parts. One term will be of the same type as for the non-regressing orbit. The other part of the solution will contain terms of the orbital regression frequency. These last terms have magnitudes dependent upon the orbital parameters and cannot, in general, be neglected. In order to keep these magnitudes low, certain tolerances are imposed on the orbital parameters. For example, for the polar orbit, the following condition is obtained:

$$\Delta\epsilon/\alpha_d = 2(-2\delta \pm .056\ i) \text{ arc sec} \qquad (2)$$

where $\Delta\epsilon$ is the satellite spin axis deviation from its original orientation, α_d is the accommodation coefficient, δ is the spin axis deviation in radians from the orbital plane, and i is the inclination in radians of the orbital plane normal to the equatorial plane. For a given $\Delta\epsilon/\alpha_d$ equation (2) establishes the tolerances for the orbital parameters δ and i.

Nondegenerate Mirror Configuration

The previously proposed mirror configuration, using mirrors identified as the facets of a truncated icosahedron, has involved a degeneracy of mirror-normal-to-spin-axis angles. For example, the choice of the normal to one of the pentagonal facets as the spin axis has involved a five-fold degeneracy, there being five facets at each angle for six angles, not counting the spin facets. Any error in fixing the spin axis, ranging from several seconds of arc to as much as 900 seconds, would provide a partial splitting of the degeneracy, partial in the sense that the glitter flash pattern would be broadened into a complicated difficult-to-analyze pattern, as described previously.[10]

The difficulty in analysis of such patterns is not one of principle, but may require the analysis of photoelectric data in addition to the photographic data, because of the limited resolution in the latter. Such analysis could prove very costly. Removal of the degeneracy could be achieved by placing the spin axis away from any facet normal by more than the 0.25^{o} (900 seconds) figure. The result could, for the same mirror configuration, be 32 different mirror angles with a five-fold reduction in the number of flashes in each pattern. While there would be a slightly more than five-fold increase in the number of opportunities (angle diversity) to make flash-pattern observations, there is some doubt as to whether the observing net could exploit this increase effectively. Also, since the individual flashes would not be resolved, this

---

[10] Prog. Report for March, April, May, 1965, p. 16, Coord. Science Lab., University of Illinois, Urbana, Illinois.

degeneracy removal would cost a five-fold reduction in photographic exposure. Such a large cost is felt to be decisive against this means of degeneracy removal

The choice of a fewer number of facets reduces the cost, in terms of a sacrifice in photographic brightness, for removing redundancy. The five-fold loss in number of facets is almost exactly made up by a slightly more than five-fold gain in individual facet area through choosing a cube of the same weight as the truncated icosahedron. There still remains the six-fold diversity of facet angles. An alternate choice would be the tetrahedron of the same weight, but with four facets each offering 80% increase in area over the individual cubic facets, but also offering only a four-fold diversity in angles. These two also have spherical figures of inertia.

A comparison in merit for these two is not altogether straightforward, however. The loss in angle diversity for the tetrahedron could be important for the proposed observation net. Also, it will undoubtedly be the case that one would want to "round-off the corners" of these figures to make the stress pattern, under high-speed rotation, conform more nearly to that for spherical objects. Such a decision will seriously damage the apparent area advantage of the tetrahedron. The choice appears to lie with the cube.

A decision to "round-off the corners" of the cube offers the opportunity to make part of the surface into a specularly reflecting sphere. This part of the surface could then be used to photograph the object at such times that the glitter flashes would not be observed,

using a tracking camera, and obtaining supplementary orbit data. Such data could be especially helpful during the early days of the experiment.

For a camera tracking with an angular speed error of ϵ percent, the effective exposure time is $(100/\epsilon)\theta r/v$, in which θ is the resolution of the camera, about 25×10^{6}m/0.5m = 5×10^{-5} radian, r is the slant range, taken to be 2500 km, and v is the orbital speed taken to be 7.5 km/sec. If the luminous flux is F at the satellite, taken to be 1.25×10^{5} lumens/m^2, then the flux at the camera is $Fd^2/16r^2$, in which d is the diameter of the sphere, taken to be 0.3m. The exposure E at the camera must be 8×10^{-11} lumen-sec/m^2 to achieve the reliable density of 0.3 to 0.4 logarithmic units above background. The required tracking accuracy is $\epsilon = (100/E) \times (\theta/v)(Fd^2/16r)$, which is 2.34%, using the above numbers. If only half the area of the body be devoted to such a spherical surface the tracking accuracy would have to be about 1.2%. One would expect this to be achievable with the help of telemetered data obtained during the launch phase.

The cost of providing such a continuous tracking facility is such as to reduce the facet area to about half what it would have been for the cube. However, it is unfair to levy all this cost against continuous tracking, since the corners of the cube would be rounded-off anyway. In addition to providing the spherical surface, it would be necessary to remove some material to provide a salient moment of inertia. The desired adjustment would involve two flats on a sphere, each having a diameter about 10% of the spherical diameter. These flats would locate the spin axis, be located on the spherical part of the surface, and

serve as spin facets, since little area is required for that function. A complete model has been worked out based on a 3-inch diameter, shown in Fig. 3.

The specifications of this model scaled to a 0.3-m diameter offer the following parameters: the spherical diameter is 30 cm; the total area of the six facets is one-half the area of the 30-cm sphere, each facet being 17.32 cm in diameter, with an area of 236 cm^2; the flat-to-flat diameter is 24.5 cm; and the angles of the mirror normals relative to the spin axis are 42, 54, and 72 degrees, with provision for two 3-cm spin facets.

To begin the calculation of photographic observability, it is interesting to calculate first the slant range at which the individual flashes begin to be resolved. For greater ranges, the photographic exposure varies inversely with the slant range. For the shorter ranges, it varies inversely with the square of the range. For a speed of 7.5 km/sec and a flash rate of 100 Hz, the flash spacing along the orbit is 75 m. This subtends an angle of 5×10^{-5} radian for a slant range of 2.5×10^{6} m or 2500 km.

At a spin rate of 100 Hz, the maximum flash duration is 7 microseconds. Using a mirror area of 236 $cm^2 = 2.36 \times 10^{-2}$ m^2, one "sees," at a slant range of 2500 km, a portion of the sun's disc through $2.36 \times 10^{-2}/(2.5 \times 10^{6})^2 = 0.38 \times 10^{-14}$ steradian. However, the sun's disc subtends 0.68×10^{-4} steradian, a reduction in luminous flux by the factor 0.56×10^{-10}. Thus, the incident flux of 1.25×10^{5} lumens/m^2 becomes, at the camera, 0.7×10^{-5} lumen/m^2. At 7 microseconds, the

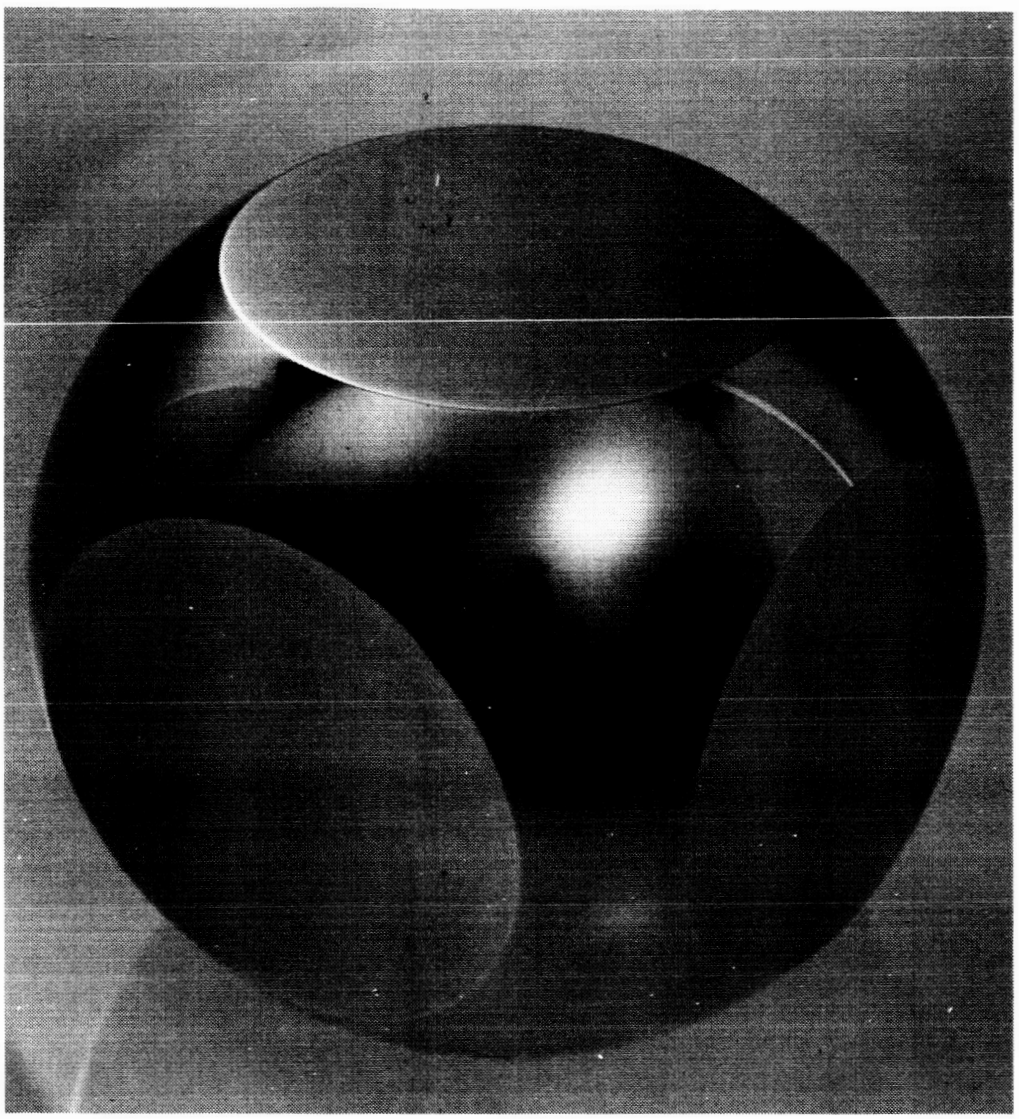

Fig. 3. Model of sphere modified by cubic-oriented flats. Half of the original area of the sphere has been used for the flats. In addition, two small flats are provided to generate a salient moment of inertia defining a spin axis. (For the model these spin facets have been fitted with bearings so that the model may be supported and spun in a yoke.) The spherical surface provides a facility for continuous orbit tracking to supplement the spin-axis tracking facility provided by the reflecting flats.

exposure is 4.9×10^{-11} lumen-sec/m^2. This is a little more than half the nominal value of 8×10^{-11} cited above.

Doubling the spin rate would reduce the resolving range by half, quadruple the light intensity, and halve the exposure time, so that the exposure would be 9.8×10^{-11} at that range, but, obeying the inverse-first-power law, fall to 4.9×10^{-11} at 2500 km. Halving the spin rate, on the other hand, would move the resolving range to 5000 km, one of no interest, but would double the exposure at 2500 km. At the same time, it would halve the number of flashes in the pattern and reduce the accuracy in estimating the center of the pattern in a way to compensate to a degree for the increased exposure for individual flashes. In this way, it is seen that the photographic effect is not very sensitive to spin rate.

The present numbers tend to suggest a definite need for a four-fold increase in facet area such as would obtain for a diameter of 0.6 m. A definitive resolution of such a question must, however, await a determination of the relation between the accuracy of measurement and the photographic exposure produced by the flash pattern.

Before turning to that discussion, it may be noted that studies involving the use of more sensitive cameras than the Baker-Nunn, or the use of a combination of photographic and photoelectric data analysis, have not yet been undertaken.

Photographic Observability and Accuracy

The basic photographic sensitivity of the Smithsonian Astrophysical Observatory's Baker-Nunn cameras, used in the above analysis

and reported previously,[11] is an important factor in the optical design of the satellite spin-axis-orientation readout system. This sensitivity needs to be interpreted, however, in terms of the accuracy with which the angular position of a flash pattern may be estimated from the Baker-Nunn photographs. Apart from errors in the measuring apparatus itself, errors in knowledge of the position of cataloged stars, and errors involving the mechanical stability of the photographic film, observation errors from a signal-to-noise competition involving film noise and a signal represented as the tapered, symmetrical density pattern of the photographed flash pattern. The latter errors may be expected to be signal-strength dependent, so that it would be important to be assured of sufficient signal strength (photographic exposure) such that the signal-dependent errors would not be appreciably larger than the instrumental errors.

The present experience is that "hard-edge" Baker-Nunn images, in which a usable density (0.3 logarithmic units or more) is developed, allow a determination in position to within about $\pm$ 1.1 seconds of arc. This number correlates well with the nominal 10 seconds-of-arc resolution for the camera, is compatible with the requirements of the relativity experiment, assuming some redundancy in observations during an undisturbed data-taking period, and it should be regarded as a goal in fixing the minimum-acceptable photographic exposure for the individual flash pattern. That minimum-acceptable exposure fixes the satellite mirror aperature;

---

[11] Prog. Report for Sept., Oct., Nov., 1965 p. 1, Coord. Science Lab., Univ. of Illinois, Urbana, Ill.

but places no bounds on the spin rate so long as more than one flash may be assured to fall within the interval of resolution of the camera.

The minimum acceptable exposure is being determined by two approaches, direct photographic simulation and computer-based simulation. In each case, it is assumed that the estimation of the image center is obtained by a weighted-average technique resembling a center-of-gravity estimation. This is illustrated schematically in Fig. 4. The upper part of the figure shows what a densitometer tracing along the long axis of a flash pattern might reveal, a roughly semicircular envelope disturbed by film noise.

Under certain circumstances, the optimal weighting procedure is known. If, for example, the noise is gaussian and uniformly additive, the best weighting curve is the derivative of the envelope. Thus, under these circumstances, a parabolic envelope would dictate a linear, or true center-of-gravity, weight, giving the most emphasis to the most steeply sloping parts of the undisturbed envelope. Optimal methods offer the advantage that approximately optimal methods are nearly indistinguishable from optimal. Under realistic circumstances, the noise will not be gaussian nor uniformly additive, and the exact envelope shape will be subject to film nonlinearities. For these reasons it is thought prudent to use the theory only as a qualitative guide, and to perform experiments with approximate weighting schemes as indicated schematically in the lower half of Fig. 4.

The dashed curve in Fig. 4 is intended to suggest what might be an optimal weight for the pattern in the upper part of that figure.

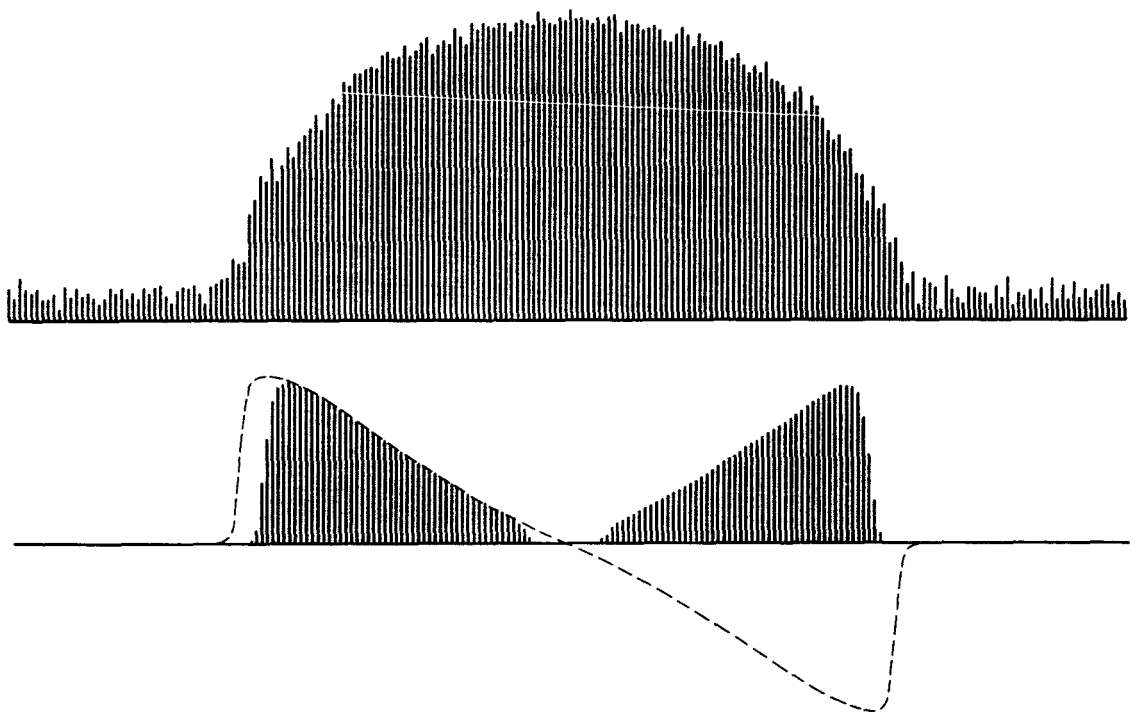

Fig. 4. Illustration of center-estimation procedure. The upper half shows, schematically, a densitometer tracing through a photograph of the expected flash pattern. A roughly semicircular envelope disturbed by the noise generated by the graininess of the film is depicted. In the lower half, a theoretically best weighting curve for finding the center (dashed line) is compared with a practical weighting scheme (bar graph) which could be realized using density wedges and balanced photometry.

Since one way to perform the weighting in practice would be to superpose density wedges upon the image, and since negative transmissions are not possible, it is proposed that two weighting functions be used, shown by the bar graphs in the lower half of Fig. 4. The two are to be exact mirror images of one another. Their relative positioning so that transmission through each is a standard amount and achieves exact equality provides the estimation of the location of the image center. Such a procedure is readily implemented in a photometric optical measuring machine that may be devised, for example, as a modification of standard apparatus. The procedure is also readily simulated in a computer.

Computer Simulation

For a computer simulation of the procedures described in connection with Fig. 4, a realistic simulation of film noise is required. Microdensitometer tracings of density step wedges,[12] made on red-extended Royal-X Pan, are being prepared for this purpose and recorded on punched paper tape. Preliminary tracings, recorded graphically were obtained using an Ansco microdensitometer through the courtesy of D. C. O'Connor[13] and transcribed to paper tape. These data were processed on a digital computer, first to prepare replicas of the original tracing using the Calcomp plotter, so that transcribing errors could be checked

[12]Courtesy of L. H. Solomon, Smithsonian Astrophysical Observatory.

[13]Geodesy, Intelligence, and Mapping Research and Development Agency, Fort Belvoir, Virginia.

and removed. Then, statistical processing resulted in a probability density histogram shown in Fig. 5, and an autocorrelation plot shown in Fig. 6.

The autocorrelation plot clearly indicates that the correlation is governed by the aperture used in the microdensitometer, 10 microns, so that the film noise has a finer structure than that. Since this is less than the 20 microns corresponding roughly to the Baker-Nunn resolution, such a resolution may be assumed for the sampling interval in the computer program, with the assurance that the noise is white relative to that. Thus, samples taken at such intervals will, in the simulation, be made to be statistically independent.

Further microdensitometer tracings will be made through the courtesy of Prof. K. Yoss of the Astronomy Department, using their Jarrel-Ash Projection Photometer, at 20 micron resolution. Probability histograms like that shown in Fig. 5 will be calculated for a variety of average densities. The computer-simulated noise will be adjusted to fit such data.

Programming of the computer simulation has begun, and some trial runs have been made. When the film noise statistics have all been obtained, so that the computer-simulated noise may be fitted to it, it will be possible to make many runs at a variety of peak-density levels and finally make a plot of measuring error versus peak density (or exposure).

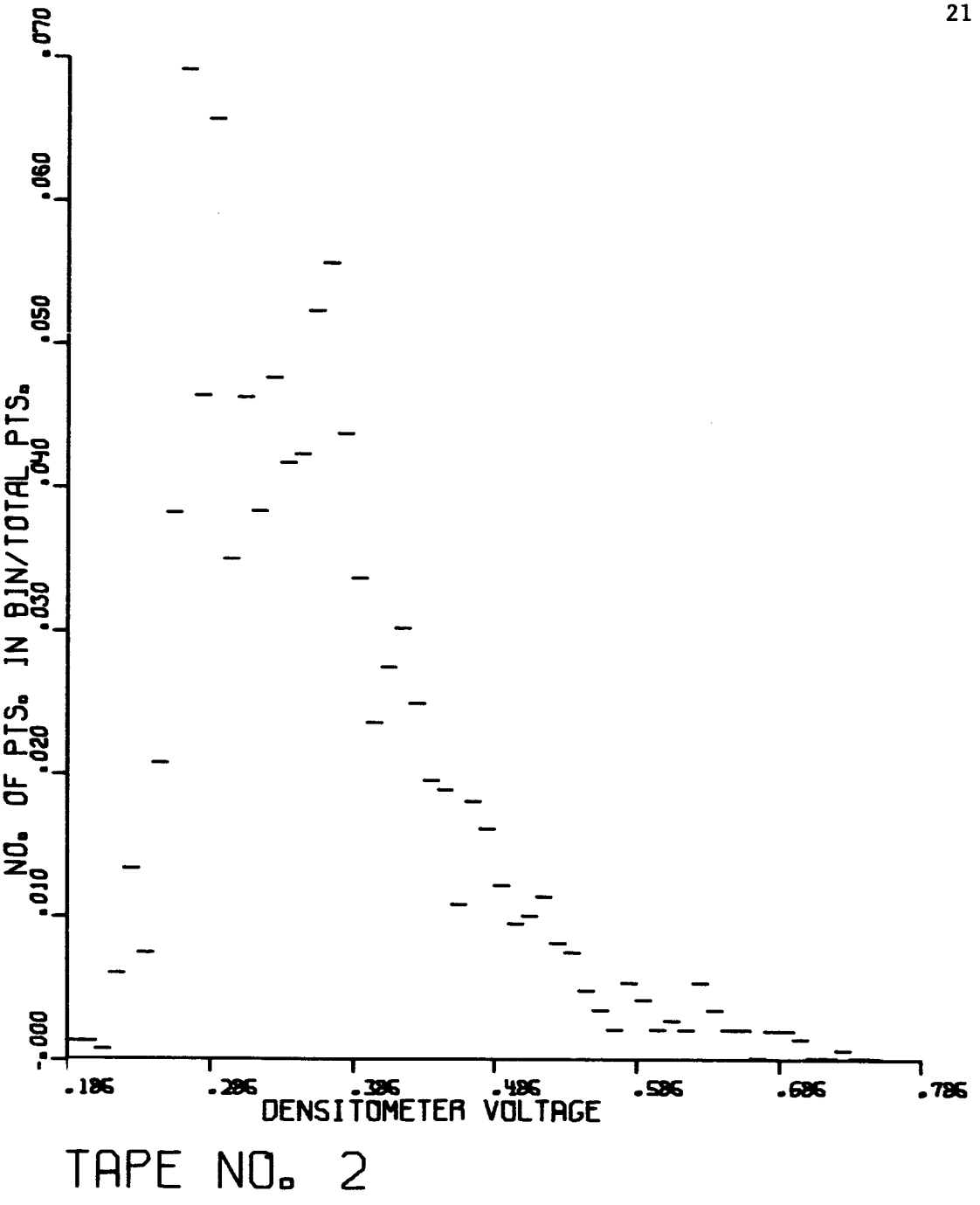

Fig. 5. Plot of probability distribution measured from a specimen of red-extended Royal-X Pan film. The "densitometer voltage" is in units of the usual logarithmic measure of density.

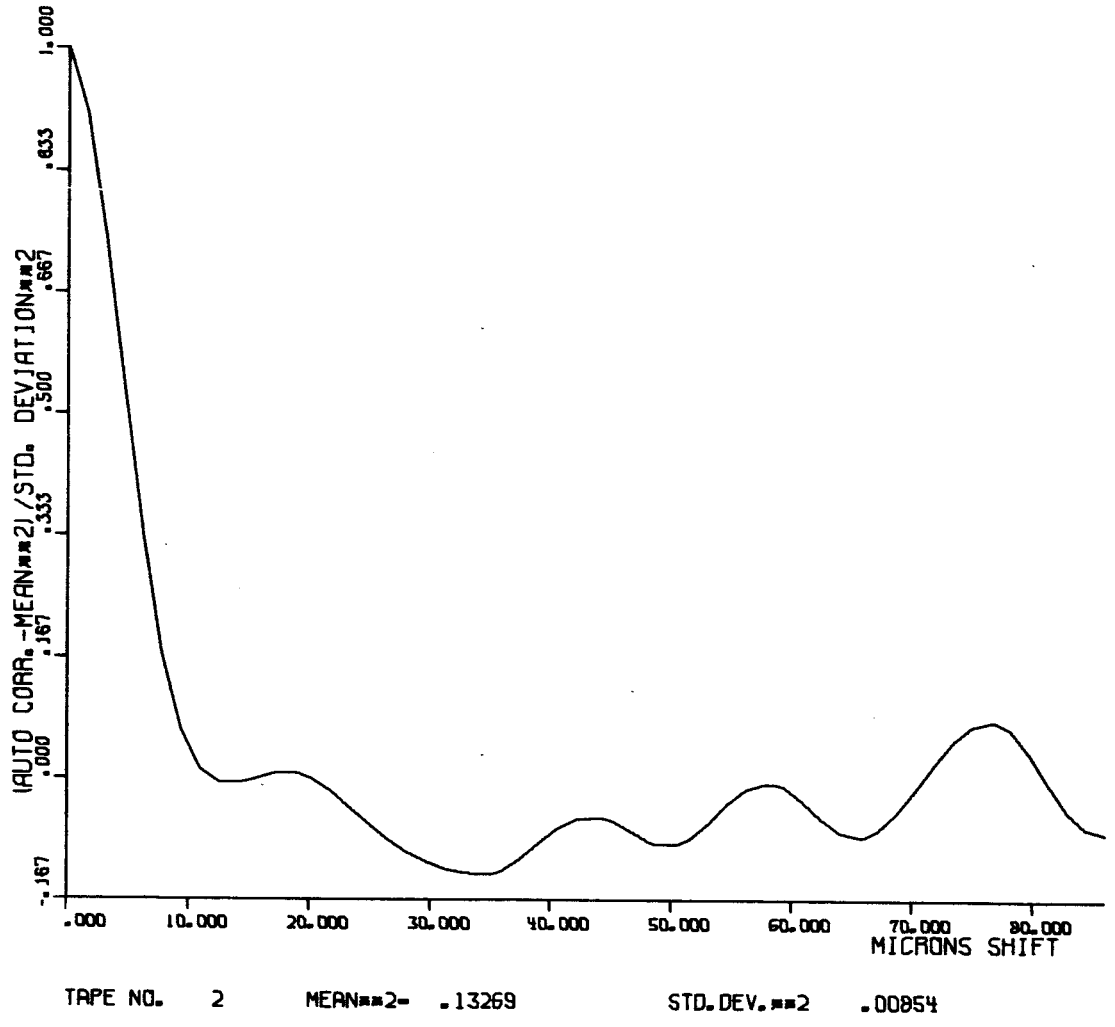

Fig. 6. Plot of the autocorrelation function for the film specimen of Fig. 3. The film-graininess noise is seen to be essentially uncorrelated at distances greater than the densitometer aperture, 10 microns.

Photographic Simulation

A cylindrical optical system has been designed by which distorted images of the sun's disc may be photographed on 35 mm red-extended Royal-X Pan film. The sun's disc will be distorted into an elliptical image with major and minor axes of about 1800 and 10 seconds of arc, respectively. For the long axis, the effective focal length of the system matches that of the Baker-Nunn camera so that the overall simulation would be to scale. The overall resolution, though not yet determined exactly, is expected to be broader than 10 seconds of arc, so that the illumination of the long, narrow image is expected to show a tapering in the long direction, which would be a realistic simulation of the brightness distribution for the glitter pattern of the satellite flashes.

The optical parts are at hand, and work has begun in fitting these parts to a Leica camera body equipped with a reflex housing. The primary optical element is a pair of convex, short focal-length cylindrical mirrors arranged so that a double image will be formed. The single objective lens is an astigmatic refractor whose cylindrical and spherical (20-inch f.l.) components complement the astigmatic properties of the cylindrical mirrors. The image is expected to be bright enough so that chromatic aberration may be controlled through the use of color filters, while the overall resolution may be controlled by adjusting the numerical aperture which will be about f:50 at widest.

It is proposed that the Jarrel-Ash projection photometer, with a specially-built dual-photomultiplier measuring station replacing the

standard one, be used to try the measuring technique outlined in an earlier section. With matching density wedges across the divided slit, and the two halves previously balanced on a uniform or blank image, the Mann measuring stage will be adjusted with the simulated image in place until balance is restored. The procedure will be repeated for the second image of the same frame. Statistics will be accumulated for the difference in measured position of the two images, for many pairs of images, and also with exposure as a parameter.